Engineering Structures 156 (2018) 598–607

Contents lists available at ScienceDirect

Engineering Structures

journal homepage: www.elsevier.com/locate/engstruct

A novel unsupervised deep learning model for global and local health condition assessment of structures

Mohammad Hossein Rafiei[a], Hojjat Adeli[b,*]

[a] Department of Civil, Environmental and Geodetic Engineering, Department of Physical Medicine Rehabilitation, The Ohio State University, 470 Hitchcock Hall, 2070 Neil Ave., Columbus, OH 43210, USA

[b] Departments of Civil, Environmental and Geodetic Engineering, Electrical and Computer Engineering, Biomedical Engineering, Neurology, and Neuroscience, The Ohio State University, 470 Hitchcock Hall, 2070 Neil Ave., Columbus, OH 43210, USA

ABSTRACT

A methodology is described for global and local health condition assessment of structural systems using ambient vibration response of the structure collected by sensors. The model incorporates synchrosqueezed wavelet transform, Fast Fourier Transform, and unsupervised deep Boltzmann machine to extract features from the frequency domain of the recorded signals. A probability density function is used to create a structural health index (SHI). This index can be used to assess both the global and local health conditions of the structure. A beauty of the proposed model is that it does not require costly experimental results to be obtained from a scaled version of the structure to simulate different damage states of the structure. Only ambient vibrations of the healthy structure are needed. In the absence of ambient vibrations, they can be simulated stochastically using structural properties and the probability theory. The effectiveness of the proposed model is illustrated employing experimental data obtained on a shake table in Hong Kong.

1. Introduction and literature review

Health monitoring of large and complex structures is considered a key high technology at the forefront of structural engineering research not only for civil structures but also aerospace and mechanical structures [3,38,39,34,35]. Significant research has been reported mostly on vibration-based health monitoring [43,34,35,19] but also on vision-based health monitoring [40]. Review of the recent literature can be found in a number of article such as Sirca and Adeli [36], Qarib and Adeli [27], Amezquita-Sanchez and Adeli [6], and Perez-Ramirez et al. [26].

Machine learning, a key technology in the 21st century, can be divided into supervised learning such as backpropagation neural networks [2], Support Vector Machine (SVM) [42,8,12], the enhanced probabilistic neural networks [4] and recently developed Neural Dynamics Classification algorithm [31] and unsupervised learning such as Self Organizing Map [7], Restricted Boltzmann machine (RBM) [37], Deep Boltzmann Machine (DBM) [17,41], and deep convolutional neural networks [11].

Recently, authors presented a new model to detect for global health monitoring of large structures such as highrise building structures based on integration of synchrosqueezed wavelet transform (SWT) [14], an unsupervised Restricted Boltzmann Machine (RBM) [37], and a new classifier developed by the authors called neural dynamics classification (NDC) algorithm [31]. The model requires experimental data on a scaled model of the structure to simulate different healthy and various damage states. The model was validated using the data obtained from a 1:20 scaled 38-story reinforced concrete building structure on a shake table in Hong Kong shown in Fig. 1a. A high maximum average accuracy of 96% was reported [30].

In this paper, a novel unsupervised learning model is presented for both global and local condition assessments of structural systems using ambient vibration response data of the structure collected by sensors. The model employs the SWT to denoise the measured signals and an unsupervised *deep* RBM (DRBM) to extract features from the frequency domain of the signals [17,29,32]. A probability density function is used to propose a structural health index (SHI) similar to development of indices for diagnosis of diseases [1]. The probability density function used in this research is derived from the concept of Bayesian inference [22,9,10] where the conditional probability of a new record of vibration given other records is computed. The conditional probability addresses the similarity of the two records known as likelihood in statistics [20].

The effectiveness of the proposed model is illustrated using the data

* Corresponding author.
E-mail addresses: rafiei.4@osu.edu (M.H. Rafiei), adeli.1@osu.edu (H. Adeli).

https://doi.org/10.1016/j.engstruct.2017.10.070
Received 11 July 2017; Received in revised form 15 August 2017; Accepted 27 October 2017
Available online 22 December 2017

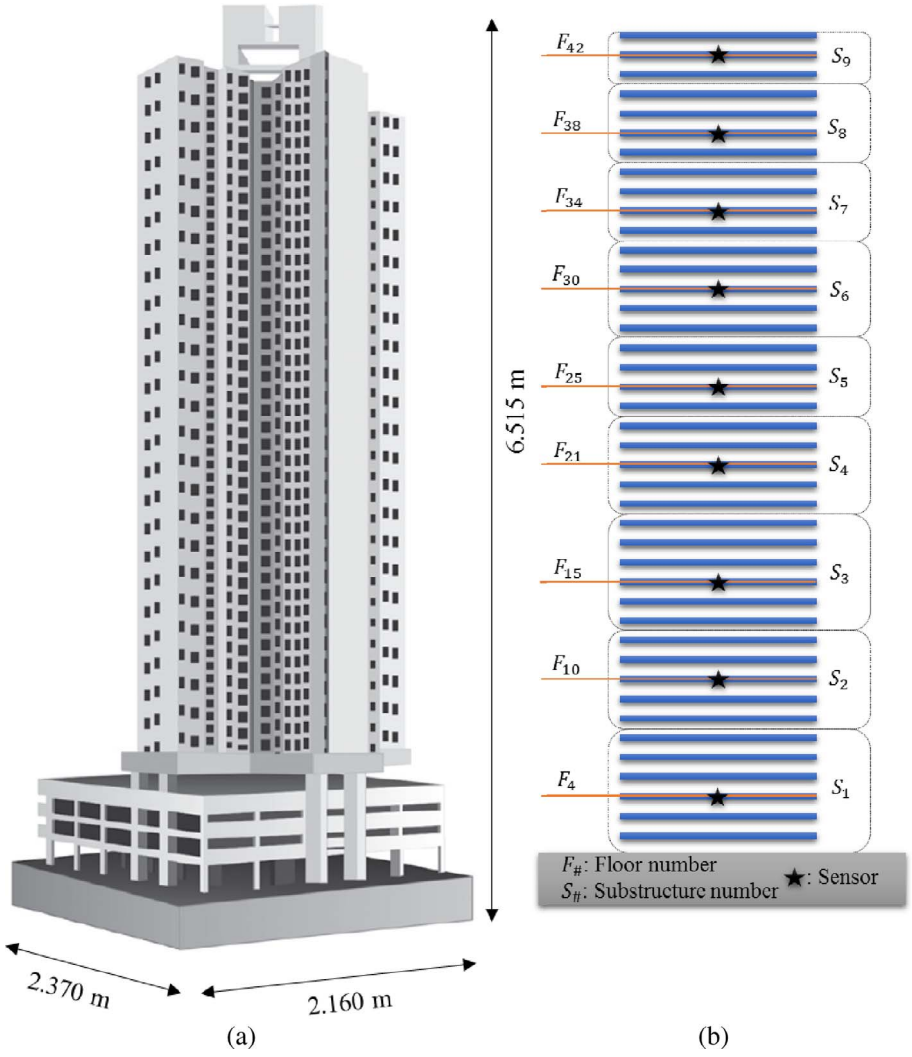

Fig. 1. (a) The scaled 38-story residential highrise building structure in Hong Kong [5,5,6]; and (b) the substructures and locations of sensors along the height.

obtained from the 3D 1:20 scaled 38-story reinforced concrete building structure [23] used in the author's earlier work [30].

2. Proposed algorithm

2.1. Requirements of the model

In contrast to the recent model developed by the authors [30], the proposed model does not require damage simulation of a scaled version of the structure. The input consists of a set of records obtained from the healthy state of the structure and another set of records with unknown health states. The model extracts information from both healthy and unknown sets to determine the health states of the unknown set. The healthy records are low-intensity ambient vibrations of the structure at least in one planar direction in the healthy state in the form of time series signals. Ambient vibrations can be due to wind, traffic, or human/pedestrian activities. Such vibrations are usually recorded by placing a few sensors on preselected locations such as floors of a highrise building structure.

The proposed model employs a substructuring scheme. Each floor of a highrise building structure and a number of its adjacent floors form a substructure. Optimum selection of substructures and sensor locations are important subjects in the field of structural system identification and health monitoring but outside the scope of the current paper. In the absence of real ambient vibrations for the healthy state, one can simulate them computationally using the probability theory. In the proposed algorithm, a structure is divided into S substructures with sensors located at least on one floor of each substructure. As an example, the 38-story reinforced concrete building structure shown Fig. 1a is divided into 9 substructures denoted as S_1, S_2, …, and S_9 with corresponding sensors located at floor numbers 4, 10, 15, 21, 25, 30, 34, 38, and 42, respectively.

2.2. Five steps performed on each substructure to calculate the local SHI

In the proposed model, 5 steps are performed for each substructure shown in Fig. 2. In step 1, first each healthy recorded time series signal of T_H seconds duration with sampling frequency of F_H Hz (totaling $T_H \times F_H$ discrete points for the signal) corresponding to a substructure is divided into N_H vectors of recorded acceleration, $\boldsymbol{H}_i$ where $i \in \{1,2,...,N_H\}$, each with $L = \frac{T_H \times F_H}{N_H}$ terms. These vectors include information about the healthy state of that substructure. Next, unknown recorded time series signal of T_U seconds duration with sampling frequency of F_U Hz (totaling $T_U \times F_U$ discrete points for the signal) corresponding to that substructure is divided into N_U vectors, $\boldsymbol{U}_j$ where $j \in \{1,2,...,N_U\}$, each with $L = \frac{T_U \times F_U}{N_U}$ terms. These vectors include information about the current unknown state of that substructure. Usually, $N_H = N_U$, $T_H = T_U$, and $F_H = F_U$. If not, N_H and N_U are selected such that $L = \frac{T_H \times F_H}{N_H} = \frac{T_U \times F_U}{N_U}$. It is postulated that with proper selection of N_H and N_U, L will be large enough such that an ample number of features is encoded and is traceable in every $\boldsymbol{H}_i$ and $\boldsymbol{U}_j$ for accurate representation of a specific healthy or damage state in a substructure.

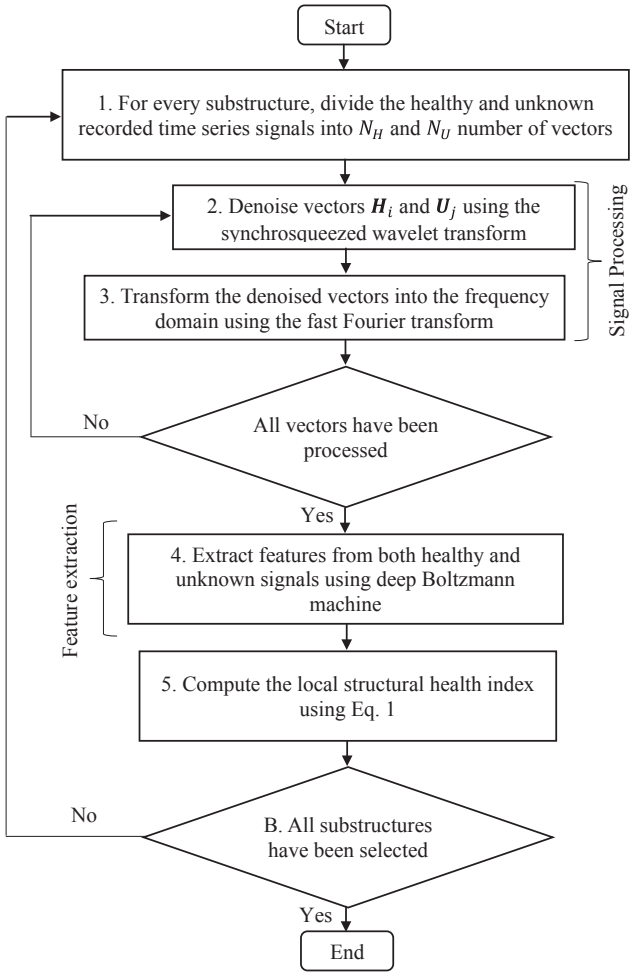

Fig. 2. Five steps of the algorithm performed on each substructure.

On the other hand, if N_H and N_U are selected such that L becomes too large, $\boldsymbol{H}_i$ and $\boldsymbol{U}_j$ may include redundant features unnecessary for accurate representation of the healthy and damage states which may make the subsequent task of feature extraction harder. But, simulation results indicate the model is not very sensitive to the variation in the size of L.

In step 2, vectors $\boldsymbol{H}_i$ and $\boldsymbol{U}_j$ are denoised using the SWT. SWT has been found to be superior to wavelet transform and discrete wavelet packet transform [24] as it employs a synchrosqueeze mapping operation [13] to include the local behavior in the time-frequency domain in the computation of the scales and time offsets [25,21]. This provides a better reconstruction at sharp points in the time domain [5].

In step 3, the denoised healthy and unknown vectors are transformed into the frequency domain using the Fast Fourier Transform (FFT) where the important characteristic of the signal is more accessible [28].

In step 4, the denoised healthy and unknown vectors transformed into the frequency domain are used as the input of a DRBM consisting of an encoder and a decoder for feature extraction (Fig. 3a). Encoder is made of several layers of restricted Boltzmann machine (RBM) intending to simulate the ability of brain to extract features from perceptions (vision, hearing, sensing, etc.). Each layer of the encoder extracts features from the extracted features of the previous layer. Hence, in general the larger the number of layers in the decoder means a larger number of extracted features cumulatively for further analysis. However, by increasing the number of layers, higher computation time is required. The number of neural network layers for proper learning and accurate feature extraction is problem-dependent and should be found based on numerical experimentation.

Decoder is symmetric to encoder intending to simulate the ability of the brain to remember and reconstruct the learned features of the perceptions. RBM is a two-layer interconnected neural network with an input layer and a hidden layer (Fig. 3b). Input and hidden layers are connected to each other through connection weights denoted by an $L \times J$ matrix $\boldsymbol{W}$ where J is the number of nodes in the hidden layer. There is no intera-connection between the neurons of a layer. RBM extracts features through an iterative procedure called constructive divergence [17]. The features common in both healthy and unknown signals are represented by the individual columns of the weight matrix, $\boldsymbol{W}$, which remains the same for healthy and the unknown records. The features that separate the two groups apart are represented by the values of the nodes in the hidden layer.

In the encoder, the hidden layer of an RBM is the input layer of the next RBM. The weights corresponding to the mth RBM, $m \in \{1,2,...,M\}$, are represented by an $L \times J_m$ matrix $\boldsymbol{W}_m$ where M is the total number of hidden layers (Fig. 3a) and J_m is the number of nodes in the mth layer of the encoder (Fig. 3b). The weights of the connections in the layers of the decoder are the transpose of the weights of the corresponding layers in the encoder denoted by an apostrophe in Fig. 3a. The last layer of the decoder is the reconstruction layer. Hinton and Salakhutdinov [17] propose a pre-training process to boost the computational efficiency and accuracy of DRBM. Details and mathematics of RBM, DRBM, encoder, decoder, constructive divergence, feature extraction, and pre-training procedure can be found in Rafiei and Adeli [29] and Rafiei et al. [32].

In step 5, a local SHI is computed for the substructure in terms of a probability density function, P, as follows:

$$R = (2\pi)^{(J_M/2)} P \tag{1}$$

$$P = \frac{1}{(2\pi)^{(J_M/2)}} \exp\left(\frac{\left\| \frac{\sum_1^{N_H} \overline{\boldsymbol{H}_i}}{N_H} - \frac{\sum_1^{N_U} \overline{\boldsymbol{U}_j}}{N_U} \right\|^2}{2} \right) \tag{2}$$

where $\overline{\boldsymbol{H}_i}$ and $\overline{\boldsymbol{U}_j}$ are the values of the hidden nodes in the last layer corresponding to $\boldsymbol{H}_i$ and $\boldsymbol{U}_j$, respectively, representing the extracted features from healthy and unknown states. Every element of $\overline{\boldsymbol{H}_i}$ and $\overline{\boldsymbol{U}_j}$ is calibrated such that the average and standard deviation of all elements in the respective vectors are 0 and 1. The terms $\frac{\sum_1^{N_H} \overline{\boldsymbol{H}_i}}{N_H}$ and $\frac{\sum_1^{N_U} \overline{\boldsymbol{U}_j}}{N_U}$ in Eq. (2) represent the vectors of averages of calibrated extracted hidden features corresponding to a healthy and an unknown signal, respectively. Hence, P can be referred to as an average probability density function. It is postulated that the healthier the structure the higher the likelihood of the unknown signal being similar to the healthy ambient signal. The larger the difference, the higher the likelihood of the damage, thus the idea behind the proposed SHI. The term $(2\pi)^{(J_M/2)}$ in Eq. (1) is used to normalize the SHI to the range 0–1. The closer the value is to 1 the healthier the structure.

2.3. Global SHI

In the previous section a local SHI was calculated for each substructure. The average of SHIs for all substructures is defined as the global SHI for the structure.

$$R_G = \frac{\sum_{s=1}^{S} R_s}{S} \tag{3}$$

where R_s is the health index of the s^{th} substructure.

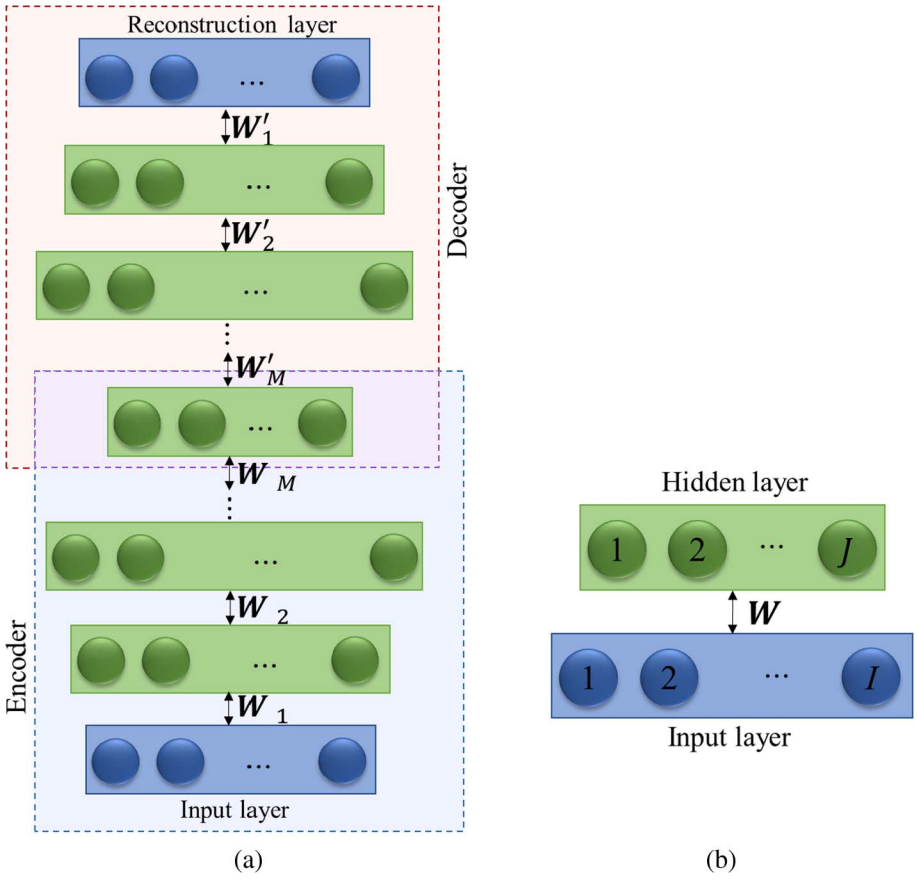

Fig. 3. (a) deep Boltzmann machine, and (b) Restricted Boltzmann machine.

3. Example application

3.1. Example and damage description

The computational model is illustrated using the shake table vibration data obtained from a 1:20 scaled residential 38-story concrete highrise building structure in Hong Kong presented schematically in Fig. 1a [23]. It consists of 3 podium floors (floor numbers 1–3), 35 residential floors (floor numbers 4–38), and 4 machine floors (floor numbers 39–42). The structure was subjected to simulated ambient, moderate, large, and very large earthquake excitations. It has been divided into 9 substructures, and equipped with 27 sensors (accelerometers). Two sensors are assigned to each substructure and placed on one floor in that substructure: floor numbers 4, 10, 15, 21, 25, 30, 34, 38, correspond to substructures 1–9, respectively. The sensors are to record the vibration of the substructures in the south–north (X direction) and east–west (Y direction). The substructures and their corresponding floors are shown in Fig. 1b.

The building first was exposed to a random white noise to record its ambient vibration response in the healthy state. A white noise simulates minor loads that do not cause damage on the structure but excites the structure similar to light wind, traffic, and human activity. Next, the building was exposed to 4 levels of earthquake excitations; (1) minor, (2) moderate, (3) strong, and (4) very strong. After each excitation, a random white noise is again applied to the building and its vibration response is recorded. Ambient vibration response of a structure after each seismic event changes. This change is captured and monitored in the proposed model to determine the damage level and calculate the SHI.

After each excitation, Ni et al. [23] monitor the structure visually to determine the extent of damage and classify into one of the four categories. After a minor earthquake, they observe very small cracks on structural members, mostly in stories 1–3 (substructure 1 in Fig. 1b). This damage state of the structure is categorized as *light damage*. After a moderate seismic event, the widths of these cracks were increased, and horizontal and diagonal cracks were observed between stories 4 and 8 (substructures 1 and 2 in Fig. 1b). This damage state is categorized as *moderate damage*. After a strong seismic event, the width of the previously appeared cracks increase. Further, around 50 new cracks, including horizontal ones, in structural and non-structural members of the middle and upper stories appear (substructure numbers 2–7 with notable new cracks on substructures 5, 6, and 7 in Fig. 1b). This damage state of the structure is categorized as *severe damage*. After a very strong seismic event, horizontal cracks were observed on the floor surfaces and some structural members were separated from the structure. This damage state of the structure is categorized as *near-collapse*.

Based on the aforementioned damage description, four damage states are defined for each substructure: A: very small to small, B: small to moderate, C: moderate to large, D: large to very large. They are summarized in Table 1.

Table 1
The extent of cracks/damage reported by Ni et al. [23] in different substructures (A: very small to small, B: small to moderate, C: moderate to large, D: large to very large).

Substructure #	Damage level			
	Light	Moderate	Severe	Near-collapse
1	A/B	A/B	C/D	D
2	A	A/B	C/D	D
3	A	B	B/C	D
4	A	B	B/C	D
5	A	B	C/D	D
6	A	B	C/D	D
7	A	B	C/D	D
8	A	B	B/C	D
9	A	B	B/C	D

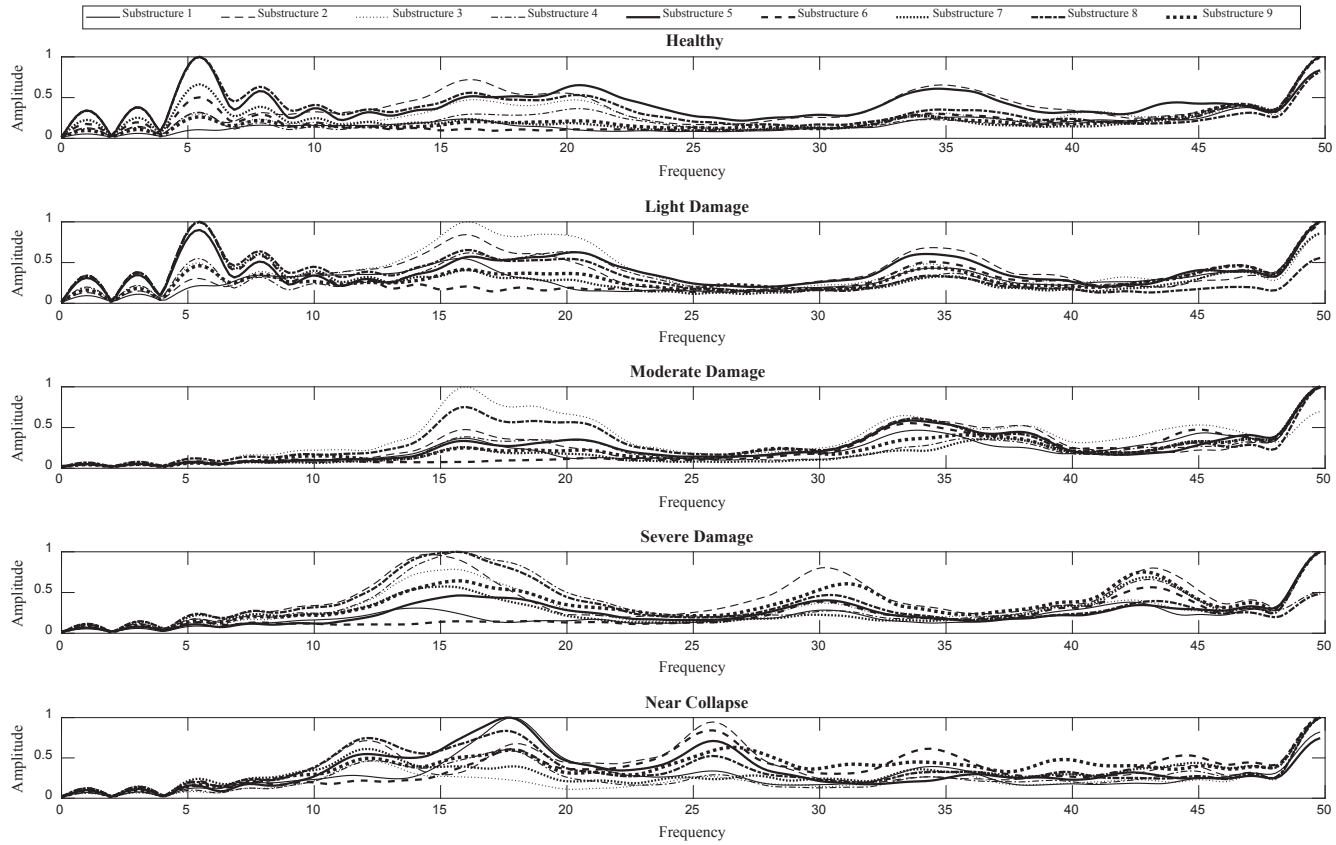

Fig. 4. The average normalized amplitude of the FFT of ambient vibrations of each substructure after the occurrence of an event in the frequency range 0–50 for five different health states (average of $N_H = N_U = 400$ values).

Table 2
The SHIs corresponding to different global and local health states for $J_2 = 2$, ($J_2 = 3$), and [$J_2 = 4$], and for $E = 2$ {$E = 10$}. Averages are shown in **(())**.

S#	Light damage	Moderate damage	Severe damage	Near-collapse
1	0.91 (0.90) [0.83]{0.91 (0.84) [0.78]} A (A) [A]{A (A) [A/B]} **((0.85)) ((A/B))**	0.92 (0.86) [0.83]{0.88 (0.80) [0.70]} A (A/B) [A/B] { A/B (A/B) [B]} **((0.83)) ((A/B))**	0.17 (0.06) [0.02]{0.16 (0.07) [0.04]} C/D (C/D) [C/D]{ C/D (C/D) [C/D]} **((0.09)) ((C/D))**	0.14 (0.04) [0.02]{0.15 (0.08) [0.04]} C/D (C/D) [C/D]{ C/D (C/D) [C/D]} **((0.08)) ((C/D))**
2	0.95 (0.96) [0.92]{0.96 (0.94) [0.91] } A (A) [A]{A (A) [A]} **((0.93)) ((A))**	0.53 (0.60) [0.54]{0.74 (0.59) [0.45]} B (B) [B]{A/B (B) [B]} **((0.49)) ((B))**	0.26 (0.18) [0.07]{0.28 (0.17) [0.11]} B/C (C/D) [C/D]{B/C (C/D) [C/D]} **((0.17)) ((C/D))**	0.17 (0.05) [0.04]{0.27 (0.14) [0.07]} C/D (C/D) [C/D]{B/C (C/D) [C/D]} **((0.13)) ((C/D))**
3	0.94 (0.96) [0.96]{0.95 (0.92) [0.86]} A(A) [A]{A (A) [A/B]} **((0.91)) ((A))**	0.83 (0.53) [0.38]{0.61 (0.46) [0.37]} A/B (B) [B/C]{B (B) [B/C]} **((0.62)) ((B))**	0.23 (0.12) [0.03]{0.24 (0.12) [0.09]} C/D (C/D) [C/D]{ C/D (C/D) [C/D]} **((0.14)) ((C/D))**	0.18 (0.08) [0.03]{0.26 (0.15) [0.09]} C/D (C/D) [C/D]{B/C (C/D) [C/D]} **((0.13)) ((C/D))**
4	0.94 (0.94) [0.88]{0.94 (0.90) [0.85]} A(A) [A/B]{A (A) [A/B]} **((0.90)) ((A))**	0.88 (0.75) [0.89]{0.84 (0.72) [0.57]} A/B (A/B) [A] {A/B (B) [B]} **((0.77)) ((A/B))**	0.16 (0.07) [0.03]{0.26 (0.11) [0.06]} C/D (C/D) [C/D]{B/C (C/D) [C/D]} **((0.11)) ((C/D))**	0.16 (0.04) [0.02]{0.25 (0.12) [0.07]} C/D (C/D) [C/D]{ C/D (C/D) [C/D]} **((0.11)) ((C/D))**
5	0.98 (0.99) [0.99]{0.99 (0.98) [0.98]} A (A) [A]{A (A) [A]} **((0.97)) ((A))**	0.76 (0.51) [0.33] {0.72 (0.54) [0.41]} A/B (B) [B/C]{B (B) [B/C]} **((0.62)) ((B))**	0.30 (0.14) [0.07]{0.35 (0.22) [0.16]} B/C (C/D) [C/D]{B/C (C/D) [C/D]} **((0.21)) ((C/D))**	0.20 (0.09) [0.03]{0.31 (0.15) [0.08]} C/D (C/D) [C/D]{B/C (C/D) [C/D]} **((0.14)) ((C/D))**
6	0.94 (0.96) [0.99]{0.99 (0.95) [0.91]} A (A) [A]{A (A) [A]} **((0.93)) ((A))**	0.38 (0.13) [0.07]{0.32 (0.18) [0.13]} B/C (C/D) [C/D]{B/C (C/D) [C/D]} **((0.23)) ((C/D))**	0.14 (0.05) [0.01]{0.31 (0.11) [0.04]} C/D (C/D) [C/D]{B/C (C/D) [C/D]} **((0.11)) ((C/D))**	0.13 (0.05) [0.01]{0.30 (0.10) [0.04]} C/D (C/D) [C/D]{ B/C (C/D) [C/D]} **((0.10)) ((C/D))**
7	0.97 (0.99) [0.97]{0.98 (0.94) [0.90]} (A) [A]{A (A) [A]} **((0.95)) ((A))**	0.67 (0.54) [0.53]{0.65 (0.53) [0.42]} B(B) [B]{B (B) [B/C]} **((0.55)) ((B))**	0.14 (0.06) [0.02]{0.25 (0.08) [0.03] } C/D (C/D) [C/D]{ C/D (C/D) [C/D]} **((0.10)) ((C/D))**	0.12 (0.09) [0.02]{0.22 (0.08) [0.03]} C/D (C/D) [C/D]{ C/D (C/D) [C/D]} **((0.08)) ((C/D))**
8	0.98 (0.99) [0.99]{0.99 (0.98) [0.96]} A (A) [A]{A (A) [A]} **((0.97)) ((A))**	0.67 (0.36) [0.22]{0.50 (0.36) [0.28] } B(B/C) [C/D]{B (B/C) [B/C]} **((0.48)) ((B))**	0.16 (0.08) [0.04]{ 0.34 (0.13) [0.06]} C/D (C/D) [C/D]{B/C (C/D) [C/D]} **((0.13)) ((C/D))**	0.16 (0.06) [0.02]{0.26 (0.10) [0.05]} C/D (C/D) [C/D]{B/C (C/D) [C/D]} **((0.11)) ((C/D))**
9	0.92 (0.89) [0.90] {0.92 (0.86) [0.81]} A (A) [A]{A (A/B) [A/B]} **((0.97)) ((A))**	0.85 (0.90) [0.69] {0.87 (0.74) [0.63]} A/B (A) [B/C]{A/B (B) [B]} **((0.76)) ((A/B))**	0.13 (0.04) [0.02] {0.17 (0.07) [0.03]} C/D (C/D) [C/D]{ C/D (C/D) [C/D]} **((0.08)) ((C/D))**	0.11 (0.05) [0.03]{0.24 (0.07) [0.03]} C/D (C/D) [C/D]{ C/D (C/D) [C/D]} **((0.08)) ((C/D))**
R_G	**0.95 (0.95) [0.94] {0.96 (0.92) [0.89] } ((0.92))**	**0.72 (0.58) [0.50] {0.68 (0.55) [0.44] } ((0.60))**	**0.19 (0.09) [0.03] {0.26 (0.12) [0.07] } ((0.13))**	**0.15 (0.06) [0.02] {0.25 (0.11) [0.06] } ((0.11))**

S#: Substructure number; A: very small to small size cracks; B: small to moderate size cracks; C: moderate to large size cracks; D: large to very large cracks.

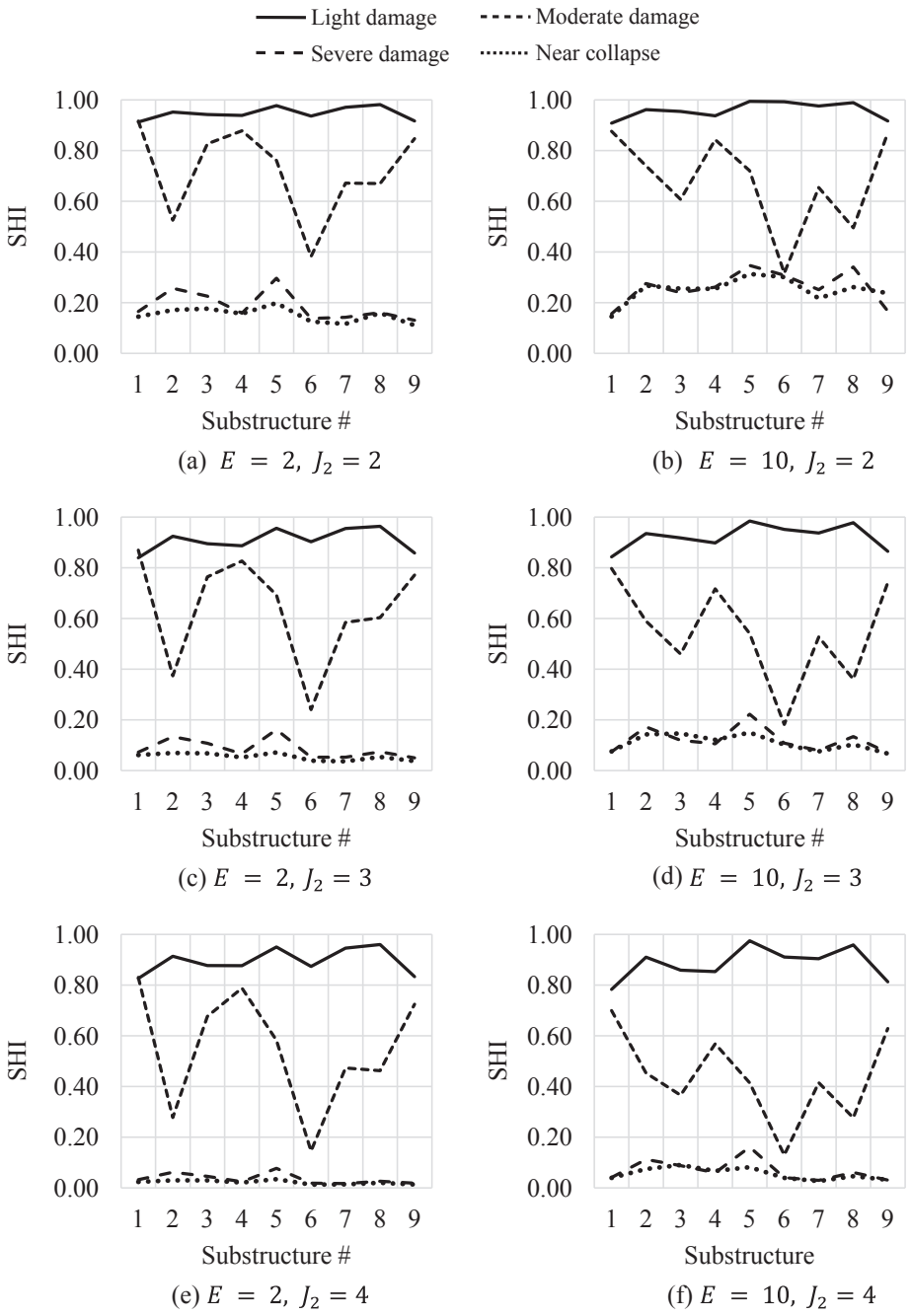

Fig. 5. Trends of SHI of each substructure corresponding to different local health states for $J_2 = 2$, $J_2 = 3$, and $J_2 = 4$, and for $E = 2$ and $E = 10$.

4. Results and discussion

The proposed model has been implemented in MATLAB. The records of ambient vibrations before and after each seismic event for 9 substructures only in the X direction are used to illustrate the model. The records other than healthy are treated as unknown records. The sampling frequency is $F_H = F_U = 100$ Hz and $T_H = T_U = 200$ s, hence, the recorded time series signal, for both healthy or unknown cases, has 20,000 values for each substructure. The proposed algorithm is used four times, each time using the record of one of the four different damage states. A value of $N_H = N_U = 400$ was found to yield accurate results. Hence the number of terms in each healthy and unknown vector is $L = \frac{200 \times 100}{400} = 50$.

Fig. 4 presents the average normalized amplitude of the FFT of ambient vibrations of each substructure after the occurrence of an event in the frequency range 0–50 for five different health states (average of $N_H = N_U = 400$ values). For each event, the shape of the curve for each substructure is similar indicating the global health state signature of the structure. The small variations reflect the local (substructure) health state of the structure. Consequently, the FFT curves can be utilized to monitor the health of the structure. In the proposed model, DRBM extracts these signatures such that the average likelihood of extracted signatures being different from those of the healthy structure increases with the increase in the damage level.

The encoder of the DRBM used for this example has just $M = 2$ layers of RBM and the hidden layer of the first RBM has $J_1 = 20$ nodes. The last layer of encoder contains $J_M = J_2$ nodes. The model is investigated for 3 values of J_2: $J_2 = 2$, $J_2 = 3$, and $J_2 = 4$. The total number of learning iterations or epochs of DRBM is denoted as E. Two values for E are investigated: $E = 2$ and $E = 10$. Hence, 6 combinations of J_2 and E are investigated for each unknown health state.

DRBM employs random initial parameters such as connection

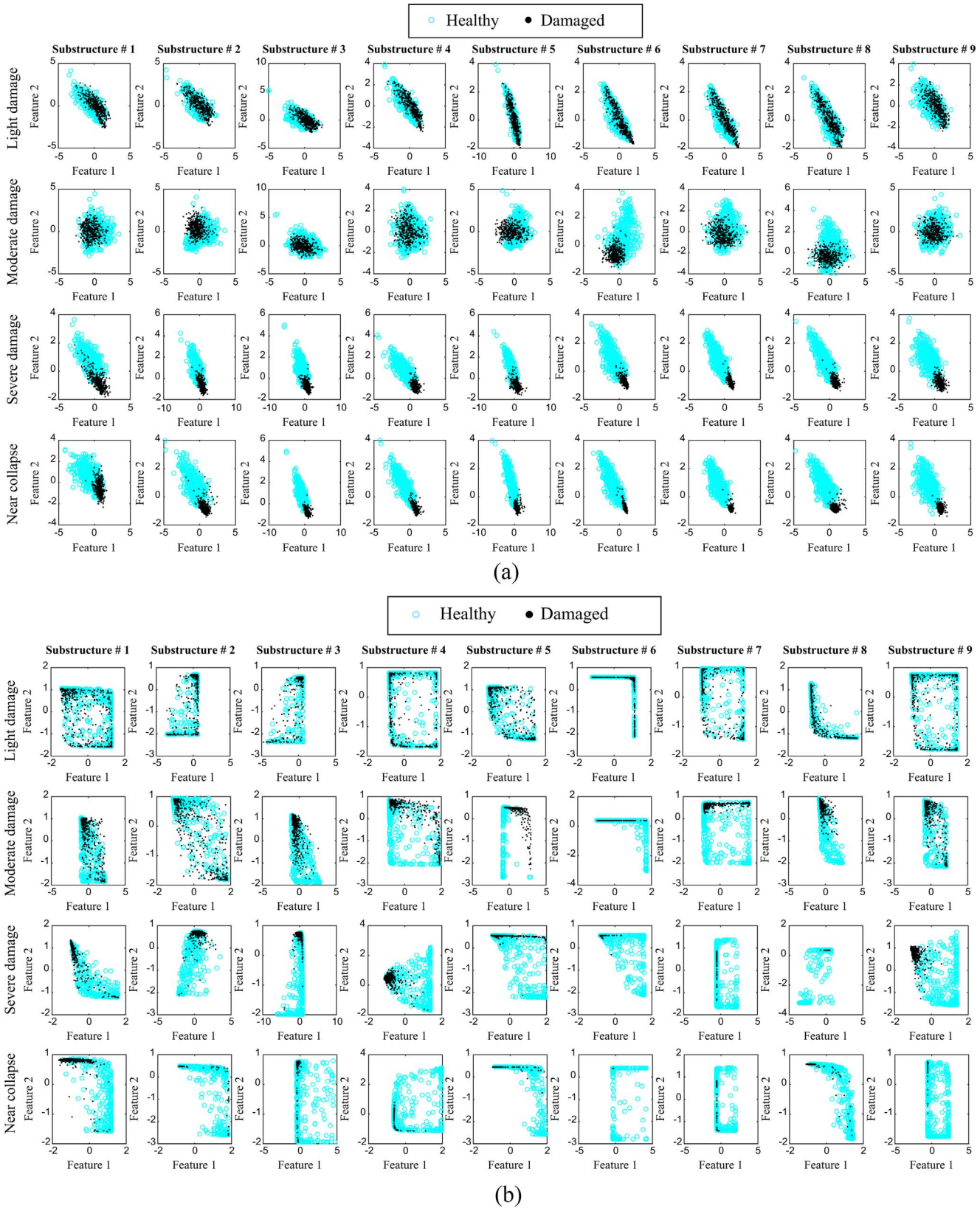

Fig. 6. Extracted features in the last layer of encoder for $J_2 = 2$ for two different values of (a) $E = 2$ and (b) $E = 10$.

weight matrices and vectors of biases. For each combination of J_2 and E, the model is run 100 times, each time using a different set of randomly selected initial parameters, and the average value is reported for SHI of each substructure.

Table 2 presents the SHIs corresponding to different global and local health states for 6 combinations of J_2 and E for each substructure for four health states where each health state is treated as an unknown health state in the model with the following notation: $J_2 = 2$, ($J_2 = 3$), and [$J_2 = 4$], and for E = 2 {E = 10}. Averages are shown in (()). Fig. 5 presents the trends of SHI of each substructure corresponding to each

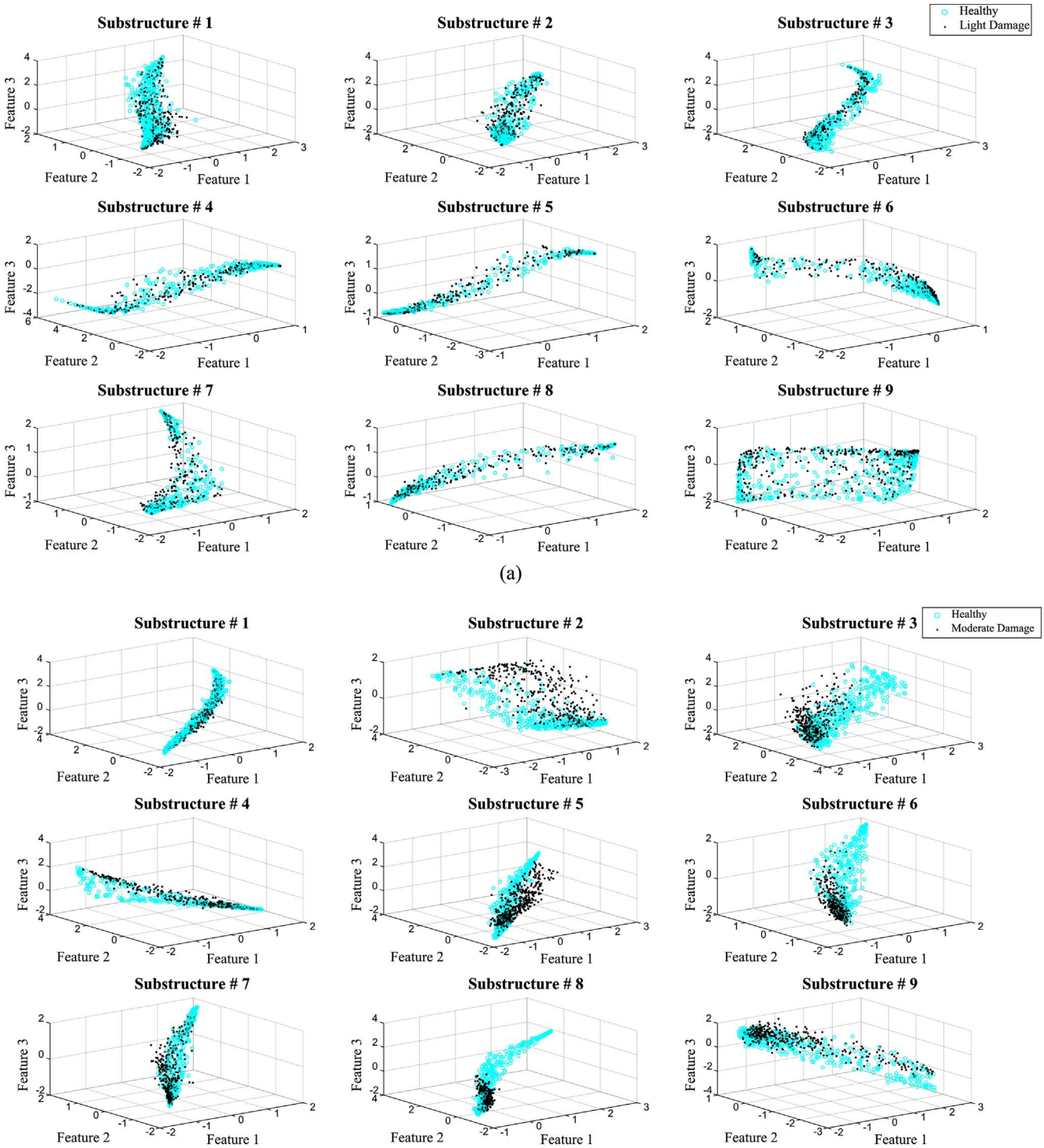

Fig. 7. Extracted features in the last layer of encoder for $J_2 = 3$ and $E = 2$ for four damage states: (a) light damage, (b) moderate damage, (c) severe damage, and (d) near-collapse.

combination. In general, for the global light damage, moderate damage, severe damage, and near-collapse structure, global SHIs of 0.89–0.96, 0.44–0.72, 0.03–0.26, and 0.02–0.25 are found, respectively. The ranges of indices of the last two categories overlap indicating the global health of severe damage and near-collapse are very similar to each other. Based on range of global health categories, authors suggest the following ranges of SHI for the 5 substructure's damage categories; 0.89–0.99 for A, 0.73–0.88 for A/B, 0.44–0.72 for B, 0.26–0.43 for B/C, and 0.00–0.25 for C/D. The corresponding substructure health categories have been shown for each combination of J_2 and E and each health state in Table 2. In Table 2, the darker the shading (color) the more severe the local damage state.

Fig. 6a and b present extracted features in the last layer of encoder for $J_2 = 2$ for two different values of $E = 2$ and 10, respectively. In these figures, each column represents a different substructure and each row represents a different damage state. Fig. 7a–d present similar results in three dimensions ($J_2 = 3$) for the four damage states. In each substructure, moving from the healthy state to higher damage states, the

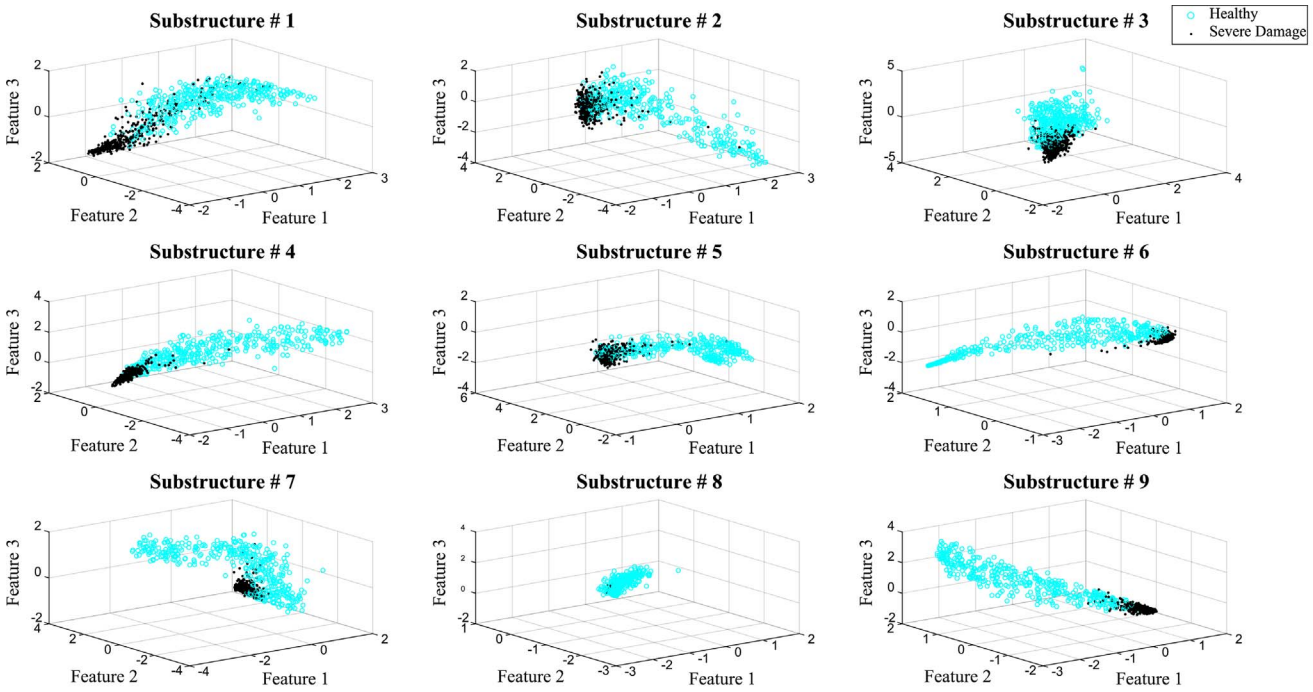

(c)

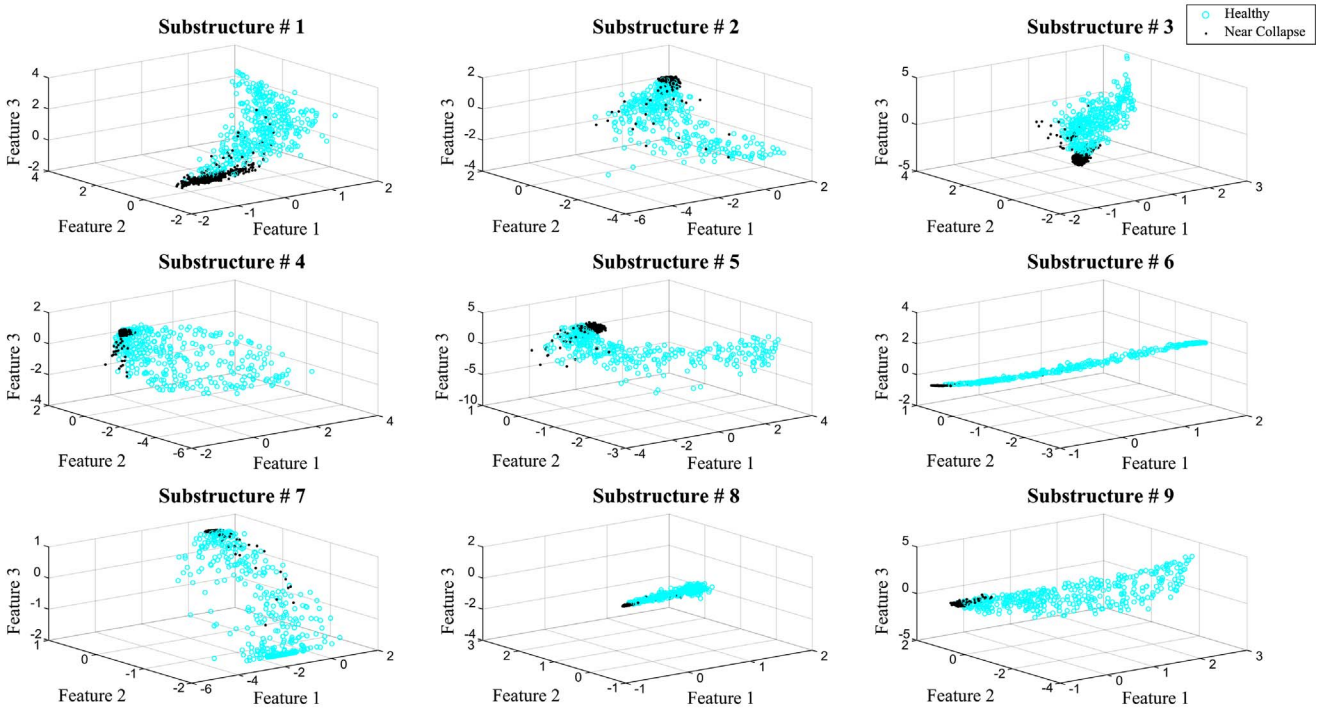

(d)

Fig. 7. (*continued*)

extracted features corresponding to the damage state (dark dots) get closer to each other and farther from those of the healthy state (light dots) and form a cluster far from the healthy features.

These features have no physical meaning and are invisible to humans in dimensions higher than 3 yet provide powerful mathematical signatures that are utilized in the proposed model adroitly to determine the health of the structure. This is the key idea in this research.

5. Conclusion

In this study, a novel algorithm is proposed for global and local health monitoring of highrise building structures using records of ambient vibration. The model has been illustrated and verified through a verification test case using actual experimental data obtained on a 1:20 scaled residential 42-story concrete highrise building structure in Hong

Kong. The records of vibration of this structure after different levels of global and local damages along with the visual inspection of the extent and severity of damages have been used to fully verify the capability of the proposed algorithm. In contrast with the previous work of the authors and many other researchers, the proposed model does not require costly experimental results to be obtained from a scaled version of the structure to simulate different damage states of the structure. Only ambient vibrations of the healthy structure are needed. The proposed model investigates the likelihood of the ambient vibrations of the current state of the structure to be similar to that of healthy structure to compute the local and global health indices. The higher the likelihood the healthier the structure. In the absence of ambient vibrations, they can be simulated stochastically using structural properties and the probability theory.

A new SHI was proposed in this research. It can be used for both local and global real-time health monitoring of structures for informed decision making for their maintenance. Authors are currently extending the model for health monitoring of bridges [15]. The authors envision the health of all the bridges of a given state to be monitored centrally continuously in real-time. The proposed SHI can be used to rank the bridges for maintenance and rehabilitation.

A frontier of research is going to be integration of health monitoring technology with active and semi-active vibration control of structures (Karami and Akbarabadi [18] to create a new generation of adaptive/smart structures.

Acknowledgment

The authors acknowledge Professor Yi-Qing Ni gratefully for providing the data for the 1:20 scaled residential 42-story concrete highrise building structure in Hong Kong.

References

[1] Acharya UR, Vidya S, Adeli H, Jayashree S, Koh JEW, Adeli A. A novel depression diagnosis index using nonlinear features in EEG signals. Eur Neurol 2015;74(1–2):79–83.
[2] Adeli H, Hung SL. Machine Learning – Neural Networks, Genetic Algorithms, and Fuzzy Systems. New York: John Wiley and Sons; 1995.
[3] Adeli H, Jiang X. Intelligent Infrastructure – Neural Networks, Wavelets, and Chaos Theory for Intelligent Transportation Systems and Smart Structures. Boca Raton, Florida: CRC Press, Taylor & Francis; 2009.
[4] Ahmadlou M, Adeli H. Enhanced probabilistic neural network with local decision circles: a robust classifier. Integr Comput-Aided Eng 2010;17(3):197–210.
[5] Amezquita-Sanchez JP, Adeli H. Synchrosqueezed wavelet transform-fractality model for locating, detecting, and quantifying damage in smart highrise building structures. Smart Mater Struct 2015;24(6):065034.
[6] Amezquita-Sanchez JP, Adeli H, 2015b. Feature extraction and classification techniques for health monitoring of structures. Scientia Iranica, – Trans A: Civil Eng 2015;22:6 [Invited Paper].
[7] Bougoudis I, Demertzis K, Iliadis L. Fast and low cost prediction of extreme air pollution values with hybrid unsupervised learning. Integ Comput-Aided Eng 2016;23(2):115–27.
[8] Castillo E, Peteiro-Barral D, Guijarro Berdinas B, Fontenla-Romero O. Distributed one-class support vector machine. Int J Neural Syst 2015;25:7, 1550029 (17 pages).
[9] Castillo A, Calviño A, Grande Z, Sánchez-Cambronero S, Gallego I, Rivas A, et al. A Markovian-Bayesian network for risk analysis of high speed and conventional railway lines integrating human errors. Comput-Aided Civil Infrastruct Eng 2016;31(3):193–218.
[10] Castillo E, Grande Z, Calviño A. Bayesian networks-based probabilistic safety analysis for railway lines. Comput-Aided Civil Infrastruct Eng 2016;31(9):681–700.
[11] Cha YJ, Choi W, Buyukozturk O. Deep learning-based crack damage detection using convolutional neural networks. Comput-Aided Civil Infrastruct Eng 2017;32(5):361–78.
[12] Chou JS, Pham AD. Smart artificial firefly colony-based support vector regression for enhanced forecasting in civil engineering. Comput-Aided Civil Infrastruct Eng 2015;30(9):715–32.
[13] Daubechies I, Maes S. A nonlinear squeezing of the continuous wavelet transform based on auditory nerve models. Wavelets Med Biol 1996:527–46.
[14] Daubechies I, Lu J, Wu H. Synchrosqueezed wavelet transforms: an empirical mode decomposition-like tool. Appl Comput Harmonic Anal 2011;30(2):243–61.
[15] Fereshtehnejad E, Hur J, Shafieezadeh A, Brokaw M. Ohio bridge condition index: multilevel cost-based performance index for bridge systems. Transport Res Record: J Transport Res Board 2017;2612:152–60.
[17] Hinton GE, Salakhutdinov RR. Reducing the dimensionality of data with neural networks. Science 2006;313(5786):504–7.
[18] Karami K, Akbarabadi S. Developing a smart structure using integrated subspace-based damage detection and semi-active control. Comput-Aided Civil Infrastruct Eng 2016;31(11):887–903.
[19] Lei Y, Zhou H, Lai ZL. A computationally compact algorithm for real-time detection of abrupt structural stiffness degradations. Comput-Aided Civil Infrastruct Eng 2016;31(6):465–80.
[20] Ley C, Bordas S. What makes data science different? A discussion involving Statistics2. 0 and Computational Sciences; 2017 http://hdl.handle.net/10993/30235 [accessed on August 14, 2017].
[21] Li Z, Park HS, Adeli H. New method for modal identification of super high-rise building structures using discretized synchrosqueezed wavelet and Hilbert transforms. Struct Des Tall Special Build 2017;26(3).
[22] Mu HQ, Yuen KV. Ground motion prediction equation development by heterogeneous Bayesian learning. Comput-Aided Civil Infrastruct Eng 2016;31(10):761–76.
[23] Ni YQ, Zhou XT, Ko JM. Experimental investigation of seismic damage identification using PCA-compressed frequency response functions and neural networks. J Sound Vibrat 2006;290(1–2):242–63.
[24] Pérez G, Conci A, Moreno AB, Hernandez-Tamames JA. Rician noise attenuation in the wavelet packet transformed domain for brain MRI. Integr Comput-Aided Eng 2014;21(2):163–75.
[25] Perez-Ramirez CA, Amezquita-Sanchez JP, Adeli H, Valtierra-Rodriguez M, Camarena-Martinez D, Romero-Troncoso RJ. New methodology for modal parameters identification of smart civil structures using ambient vibrations and synchrosqueezed wavelet transform. Eng Appl Artif Intell 2016;48:1–12.
[26] Perez-Ramirez CA, Amezquita-Sanchez JP, Adeli H, Valtierra-Rodriguez M, Romero-Troncoso RJ, Dominguez-Gonzalez A, et al. Time-frequency techniques for modal parameters identification of civil structures from acquired dynamic signals. J Vibroeng 2016;18(5):3164–85. http://dx.doi.org/10.21595/jve.2016.17220.
[27] Qarib H, Adeli H. Recent advances in health monitoring of civil structures. Scientia Iranica-TransA: Civil Eng 2014;21(6):1733–42.
[28] Qarib H, Adeli H. A new adaptive algorithm for automated feature extraction in exponentially damped signals for health monitoring of smart structures. Smart Mater Struct 2015;24(12):125040.
[29] Rafiei MH, Adeli H. A novel machine learning model for estimation of sale prices of real estate units. J Constr Eng Manage 2015;142(2):04015066.
[30] Rafiei MH, Adeli H. A novel machine learning-based algorithm to detect damage in high-rise building structures. Struct Des Tall Spec Build 2017:e1400-n/a.
[31] Rafiei MH, Adeli H. A New Neural Dynamic Classification Algorithm. IEEE Trans Neural Networks Learn Syst 2017;PP(99):1–10.
[32] Rafiei MH, Khushefati WH, Demirboga R, Adeli H. Supervised deep restricted boltzmann machine for estimation of concrete. ACI Mater J 2017;114(2).
[34] Shan J, Ouyang Y, Yuan HW, Shi W. Seismic data driven identification of linear physical models for building structures using performance and stabilizing objectives. Comput-Aided Civil Infrastruct Eng 2016;31(11):846–70.
[35] Shan J, Shi W, Lu X. Model reference health monitoring of hysteretic building structure using acceleration measurement with test validation. Comput-Aided Civil Infrastruct Eng 2016;31(6):449–64.
[36] Sirca GF Jr, Adeli H. System identification in structural engineering", Scientia Iranica – Transaction A: Civil Engineering 2012;19:6 1355–1364 [Invited Paper].
[37] Smolensky P. Information processing in dynamical systems: foundations of harmony theory. In: Chapter Six in Rumelhart DE, McClelland JL, the PDP Research Group, editors, Parallel Distributed Processing – Volume 1 Explorations in the Microstructure of Cognition: Foundations, MIT Press, Cambridge, MA; 1986.
[38] Tondini N, Bursi OS, Bonelli A, Fassin M. Capabilities of a fiber Bragg grating sensor system to monitor the inelastic response of concrete sections in new tunnel linings subjected to earthquake loading. Comput-Aid Civil Infrastruct Eng 2015;30(8):636–53.
[39] Wandowski T, Malinowski P, Ostachowicz W, Luba T, Borowik G, Rawski M, et al. Embedded damage localization subsystem based on elastic wave propagation. Comput-Aided Civil Infrastruct Eng 2015;30(8):654–65.
[40] Yeum CM, Dyke SJ. Vision based automated crack detection for bridge inspection. Comput-Aided Civil Infrastruct Eng 2015;30(10):759–70.
[41] Zhang A, Fei Y, Wang KCP, Li B, Liu Y, Li JQ, et al. Automated pixel-level pavement crack detection on 3D asphalt surfaces using a deep-learning network. Comput-Aided Civil Infrastruct Eng 2017;32:10.
[42] Zhang Y, Zhou W. Multifractal analysis and relevance vector machine-based automatic seizure detection in intracranial. Int J Neural Syst 2015;25:6, 1550020 (14 pages).
[43] Zhong Y, Xiang J. A two-dimensional plum-blossom sensor array-based multiple signal classification method for impact localization in composite structures. Comput-Aided Civil Infrastruct Eng 2016;31(8):633–43.Further reading
[16] Gilles J. Empirical wavelet transform. IEEE Trans Signal Process 2013;61(16):3999–4010.
[33] Sankari Z, Adeli H. Probabilistic neural networks for diagnosis of Alzheimer's disease using conventional and wavelet coherence. J Neurosci Methods JID 2011;7905558(1872–678).